EBioMedicine 2 (2015) 386–395

Contents lists available at ScienceDirect

EBioMedicine

journal homepage: www.ebiomedicine.com

Original Article

Unraveling the Activation Mechanism of Taspase1 which Controls the Oncogenic AF4–MLL Fusion Protein

Samaneh Sabiani [a], Tim Geppert [b], Christian Engelbrecht [a], Eric Kowarz [a], Gisbert Schneider [b], Rolf Marschalek [a,*]

[a] Institute of Pharmaceutical Biology, Goethe-University of Frankfurt, Biocenter, Max-von-Laue-Str. 9, D-60438 Frankfurt/Main, Germany
[b] Institute of Pharmaceutical Sciences, ETH Zurich, Wolfgang-Pauli-Str. 10, 8093 Zurich, Switzerland

ARTICLE INFO

Article history:
Received 19 November 2014
Received in revised form 14 April 2015
Accepted 14 April 2015
Available online 16 April 2015

Keywords:
t(4;11) leukemia
Taspase1
AF4–MLL
Oncoprotein activation

ABSTRACT

We have recently demonstrated that Taspase1-mediated cleavage of the AF4–MLL oncoprotein results in the formation of a stable multiprotein complex which forms the key event for the onset of acute proB leukemia in mice. Therefore, Taspase1 represents a conditional oncoprotein in the context of t(4;11) leukemia. In this report, we used site-directed mutagenesis to unravel the molecular events by which Taspase1 becomes sequentially activated. Monomeric pro-enzymes form dimers which are autocatalytically processed into the enzymatically active form of Taspase1 ($\alpha\beta\beta\alpha$). The active enzyme cleaves only very few target proteins, *e.g.*, MLL, MLL4 and TFIIA at their corresponding consensus cleavage sites (CS_{Tasp1}) as well as AF4–MLL in the case of leukemogenic translocation. This knowledge was translated into the design of a dominant-negative mutant of Taspase1 (dnTASP1). As expected, simultaneous expression of the leukemogenic AF4–MLL and dnTASP1 causes the disappearance of the leukemogenic oncoprotein, because the uncleaved AF4–MLL protein (328 kDa) is subject to proteasomal degradation, while the cleaved AF4–MLL forms a stable oncogenic multi-protein complex with a very long half-life. Moreover, coexpression of dnTASP1 with a BFP-CS_{Tasp1}-GFP FRET biosensor effectively inhibits cleavage. The impact of our findings on future drug development and potential treatment options for t(4;11) leukemia will be discussed.

1. Introduction

The chromosomal translocation t(4;11) results from an illegitimate recombination event that involves both the *MLL/KMT2A* (11q23) and *AF4/AFF1* (4q21) gene. Such genetic aberrations are frequently diagnosed in early childhood and pediatric acute leukemia patients (Meyer et al., 2009). Despite all the improvements over the past decades, the current treatment regimen for these patients — mainly if the disease occurs within the first year of life — results in poor outcome. Genetic rearrangements of *MLL* and *AF4* are mostly caused by balanced chromosomal translocations, resulting in the creation of two fusion genes, *MLL–AF4* and *AF4–MLL*, respectively. Both fusion alleles are detected in about 80% of t(4;11) leukemia patients, while 20% of t(4;11) leukemia patients exhibit complex rearrangements with three or more fusion genes (Kowarz et al., 2007). Moreover, it was recently demonstrated that both reciprocal t(4;11) fusion proteins give rise to leukemia development in the murine system: (1) expression of an *Mll–AF4* fusion protein in a transgenic knock-in mouse strain resulted in the development of AML and ALL (Krivtsov et al., 2008); (2) retroviral expression of the AF4–MLL fusion protein alone resulted in the development of proB ALL in mice (Bursen et al., 2010). Noteworthy, a recent study has demonstrated that MLL–AF4 causes an increased expression of RUNX1 which promotes the onset of leukemia for the case of AF4–MLL translocation (Wilkinson et al., 2013).

To become oncogenic AF4–MLL requires a prior endoproteolytic cleavage mediated by Taspase1 (Bursen et al., 2004). Taspase1 was discovered as a sequence-specific endopeptidase that hydrolyzes the MLL protein at two cleavage sites, CS1 and CS2, both localized within the C-terminal portion of the MLL protein. Enzymatic hydrolysis of MLL occurs between amino acid positions 2666/2667 and 2718/2719 (Hsieh et al., 2003a,b). Subsequently, the resulting MLL protein fragments ($p320^N$ and $p180^C$) dimerize and form a high molecular weight complex. This MLL multi-protein complex carries out important epigenetic functions ($H3K4_{me3}$; $H4K16_{Ac}$; H_{Ac}) that are directly linked to transcriptional maintenance (Nakamura et al., 2002; Yokoyama et al., 2004; Dou et al., 2005). All of these functions are carried out in a transcription factor dependent fashion (MENIN1, LEDGF and c-MYB) (Yokoyama et al., 2004; Yokoyama and Cleary, 2008; Jin et al., 2010),

* Corresponding author at: Institute of Pharmaceutical Biology, University of Frankfurt, Max-von-Laue-Str. 9, 60438 Frankfurt/Main, Germany.
E-mail address: Rolf.Marschalek@em.uni-frankfurt.de (R. Marschalek).

http://dx.doi.org/10.1016/j.ebiom.2015.04.009

targeting about 2000 genes in the mammalian genome (Guenther et al., 2005). Moreover, the MLL complex regulates developmental and differentiation processes, and is required for the normal development of the hematopoietic system (Ono et al., 2005; Jude et al., 2007; McMahon et al., 2007; Gan et al., 2010).

Taspase1 represents a highly unique enzyme that has co-evolved in vertebrates and invertebrates together with proteins of the Trithorax/MLL family. The crystal structure of Taspase1 has already been revealed (PDB-ID: 2A8I, 2A8J, 2A8J) (Khan et al., 2005). According to these structures, two monomeric Taspase1 proenzymes (p50) form a homodimer (p50/p50) that are subsequently processed into two α-(amino acids 1–233; p28) and two β-subunits (234–420; p22), both of which remain stably associated (αββα). Importantly, the β-subunit carries the N-terminal threonine-234 residue (T234), which represents the catalytic center (Khan et al., 2005). Thus, a Taspase1 homodimer exhibits two catalytic centers that are oriented in an angle of about 108° at opposing sides of the dimer. Both catalytic centers contain a single chloride ion that is part of an intrinsic regulatory mechanism and inhibits Taspase1 at physiological sodium chloride concentrations (IC_{50} ~ 25 mM NaCl) (Khan et al., 2005; Michalska et al., 2006). The target consensus sequence hydrolyzed by Taspase1 is $Q^3[F,I,L,V]^2D^1|G^{1'}X^{2'}X^{3'}D^{4'}$, but only MLL, MLL4 and TFIIA as well as the oncogenic AF4–MLL fusion protein are confirmed substrates (Bursen et al., 2004; Hsieh et al., 2003b; Zhou et al., 2006).

For the AF4–MLL fusion protein the Taspase1-induced protein fragments ($p178^N$ and $p180^C$) heterodimerize *via* specific domains localized in both protein fragments (FYRN and FYRC) (Yokoyama et al., 2002; Hsieh et al., 2003a). After dimerization, a multi-protein complex is formed that exerts strong oncogenic activities: a) ectopic activation of P-TEFb kinase results in a hyperactivation of transcriptional elongation processes, and b) co-bound histone methyltransferases cause ectopic H3K4/H3K79 patterns which subsequently effectuate epigenetic deregulation in a genome-wide fashion (Benedikt et al., 2011). Without the fragment dimerization both AF4–MLL fragments are subject to proteasomal destruction (Pless et al., 2011).

Since Taspase1 processing of AF4–MLL is essential for its oncogenic action, we investigated structure–function relationships of human Taspase1. Using site-directed mutagenesis in combination with functional experiments, we were able to demonstrate that dimerization of two Taspase1 proenzymes is a prerequisite for the autoproteolytic processing of Taspase1 into the necessary α- and β-subunits. Based on our results, we designed a dominant-negative Taspase1 variant that prevents the dimerization of AF4–MLL fragments and induces the proteasomal degradation of the AF4–MLL. Moreover, modified cells are unable to activate a FRET reporter. The relevance of these findings for future cancer therapy will be discussed.

2. Methods

2.1. Modeling of Taspase1

Comparative protein ('homology') modeling of Taspase1 was performed by examining available protein templates. Four different crystallographic structures of Taspase1 were available from the Protein Data Bank (PDB IDs: 2A8I, 2A8J, 2A8L, 2A8M) (Khan et al., 2005; Michalska et al., 2006). PDB structure 2A8J (chain A) served as the template for construction of a homology model of activated Taspase1. One structural element (sequence positions 164–180) was modeled based on the established structure of another glycosylasparaginase (PDB ID: 1P4K), which has a sequence identity of 29% to Taspase1. The whole multi-template modeling process was executed within the homology modeling software package MODELLER 9v3 (Eswar et al., 2006). The resulting protein structural model was evaluated using PROCHECK (Laskowski et al., 1993). The Ramachandran plot shows that 92.3% of all residues are located within favored regions (Suppl. Fig. S2). Based on this observation we decided not to further minimize the model. The Taspase1 model structure was duplicated and aligned to both chains of the complex in PDB structure 2A8J using the 'align' function of the PyMOL software package (Version 1.3, Schrödinger, LLC).

2.2. In Vitro Taspase1 Cleavage Assay

The cDNA of human Taspase1 was cloned into the pET22b expression plasmid and recombinantly expressed in *E. coli* strain BL21* (Invitrogen, Darmstadt, Germany). An appropriate MLL substrate was constructed by cloning a cDNA fragment of MLL comprising amino acids 2614–2773 into the pGEX-5T expression vector. The resulting GST–MLL fusion protein (p50) exhibits the CS1 (QVD·GADD) and CS2 (QLD·GVDD) sites for hydrolysis by Taspase1. Expression of the C-terminal His-tagged Taspase1 protein and the N-terminal His-tagged GST–MLL fusion protein (p50) was induced by adding 1 mM IPTG for 4 h, followed by Ni-NTA affinity-purification following the instructions of the manufacturer (Sigma, Munich, Germany). For *in vitro* cleavage assays, equal amounts of purified Taspase1 and GST–MLL substrate protein (~0.5 μg protein) were co-incubated in incubation buffer containing 40 mM Hepes/KOH pH 7.9, 10 mM KCl and 5 mM $MgCl_2$ for 30 min at 37 °C. Enzyme, substrate and hydrolyzed products were separated on a 12% SDS-PAGE and Coommassie blue-stained for visual inspection.

2.3. Site-directed Mutagenesis of Taspase1

Site-directed mutagenesis of Taspase1 and the GST–MLL substrate protein was performed using a commercially available mutagenesis kit (Agilent Technologies, Böblingen, Germany) in combination with specific oligonucleotides that are listed in Suppl. Table S1.

2.4. Testing the Dimerization Capacity of Different Taspase1 Mutants

Dimerization between Taspase1 variants was tested using a mammalian expression vector (pCDNA; Invitrogen, Darmstadt, Germany) that contain Taspase1 (or its mutated variants) fused either to a C-terminal Flag- or Myc-Tag (Hopp et al., 1988; Evan et al., 1985). Corresponding plasmids (Flag and Myc) containing either the mutated Taspase1 variant or the combination of mutated Taspase1 variant and wildtype Taspase1 were co-transfected into 293T cells for co-immunoprecipitation experiments. Immunoprecipitation was always performed using an anti-Flag Tag antibody (clone M2; Sigma, Munich, Germany), while detection of dimerized Taspase1 was confirmed in Western blot experiments by using an anti-Myc Tag antibody (clone 9E10; Abcam, Cambridge, UK).

2.5. Cell Growth, Western Blot and Q-PCR Experiments

HEK293T were transfected with expression constructs for wildtype Taspase1::Flag and the dnTASP1::Flag mutant variant in conjunction with an AF4–MLL expression plasmid. SEM cells were stably transfected with an inducible dnTasp or Luciferase expression constructs. Transfected cells were selected with Puromycin and nearly 100% pure cultures were used for all experiments, *e.g.*, for cell growth experiments. Total cell lysates were prepared and used for Western blot experiments. For the detection of β-actin, the polyclonal antiserum #4967 (Cell Signaling, Schwalbach/TS, Germany) was used. Similarly, stably transfected cells were used to prepare total RNA that was subsequently used for quantitative PCR experiments (n = 3). Appropriate primers for the quantification of transcripts derived from the *HOXA1*, *HOXA3*, *HOXA7*, *HOAX9* and *HOXA10* genes were designed. The following primers were used: HOXA1·3 (5′-acagaacttcagtgcgccttaca-3), HOXA1·5 (5′-gggagcgacaggcttcttg-3′), HOXA7·3 (5′-agcttggaaattctgctcacttct-3′), HOXA7·5 (5′-tctgatgtca tggccaaatttg-3′), HOXA9·3 (5′-gccggccttatggcattaa-3′), HOXA9·5 (5′-cagggacaaagtgtgagtgtcaa-3′), HOXA10·3 (5′-aaagcctcgccggagaa-3′)

and HOXA10·5 (5′-ctccagtgtctggtgcttcgt-3′). All quantitative PCR reactions were performed in triplicates and normalized against PDK1 using the following primer set: PDK1·3 (5′-gagagtcgacttcaagttc-3′) and PDK1·5 (5′-gtccttcaagaacagacat-3′).

2.6. In Vivo FRET Assay

The FRET biosensor reporter consists of a TagBFP/TagGFP FRET pair separated by either of the 2 Taspase1 cleavage sites CS1 (AEGQVDGADD) or CS2 (KISQLDGVDD), respectively. This FRET biosensor was stably co-transfected with either wild-type Taspase1, dnTASP1 or empty vector (mock) by using a Sleeping Beauty vector system (Wächter et al., 2014). All Taspase1 constructs or the mock vector co-expresses RFP (dTomato) that was used for normalization. Transfections were carried with the 2 different Taspase1 vectors or mock, the FRET biosensor reporter vector and SB100X transposase plasmid (Mátés et al., 2009) and then selected in the presence of either Puromycin (3 μg/ml; FRET biosensor vector) and Blasticidin (10 μg/ml, Taspase1 vectors/mock). Stable cell lines were obtained within 5–10 days. Biosensor cleavage was measured *via* BFP quenching in the living cells. BFP fluorescence (Ex: 402 nm; Em: 457 nm) of 50,000 cells was measured with a Thermo Scientific Varioskan Flash plate reader (n = 12). The fluorescence was normalized to the dTomato fluorescence (Ex: 554 nm; Em: 581 nm) deriving from the Taspase1/mock vectors.

3. Results

3.1. Structural Modeling of Taspase1

The currently available crystal structure information on Taspase1 contains several unstructured regions that have not been resolved or assigned (Khan et al., 2005). Amino acids 1–40, 206–229 and 352–362 are missing in PDB records 2A8I and 2A8J, respectively (Fig. 1, left panel). The PDB structure 2A8J (chain A, active Taspase1) was chosen to serve as the principal template for modeling of a full Taspase1 structure. The pair-wise alignment with the template contains a total of 66 gap positions. Missing residues belong to three continuous gaps. The lengths of the three gaps are two, 50, and 14 amino acids. Missing residues were modeled based on three different protein structures. Based on Taspase1 structure 2A8I (chain B) we modeled ten residues of the 14-residue gap, while the remaining residues were modeled *de novo*. Using the Taspase1 structure 2A8I (chain A, Taspase1 proenzyme) we reconstructed the two-residue gap as well as 25 residues of the 50-residue gap. Twenty-four of the 25 remaining gap residues were modeled based on the established protein structure of glycosylasparaginase (1P4K, chain C) (Qian et al., 2003), while one residue was modeled *de novo*. As shown in Fig. 1 (right panel), the missing residues 206–229 and 352–362 form additional structural elements (shown in red). Sequence positions 164–180 were modeled based on the established structure of another glycosylasparaginase (PDB ID: 1P4K); this resulted in conformational changes of regions in positions 153–167 and 189–205 (also depicted in red).

3.2. Establishment of an In Vitro Taspase1 Hydrolysis Assay

Recombinant human Taspase1 and a GST–MLL substrate protein (consisting of the *E. coli* GST protein fused to about 150 amino acids deriving from the human MLL protein and containing the two cleavage sites CS1 and CS2) were expressed and affinity-purified using a C- and N-terminal His-tag, respectively. In all Taspase1 preparations, the full-length proenzyme (p50) co-purified along with equal amounts of the autoproteolyzed protein fragments of Taspase1 (p28 & p22). This indicated that the intrinsic Taspase1 autoproteolysis did not impair the affinity-purification step. Protein preparations were subsequently used for an *in vitro* hydrolysis assay. For each preparation, an SDS-PAGE was performed to test the enzymatic activity of purified Taspase1. An example is presented in Fig. 2, where decreasing amounts of a Taspase1 preparation were used in combination with a constant amount of the substrate protein (ratios between Taspase1 and GST–MLL are 1:1 up to 1:128). Cleavage of the substrate protein was most efficient at a 1:1 ratio between Taspase1 and substrate protein. Therefore, all subsequent *in vitro* proteolysis assays were performed with equimolar quantities of recombinant Taspase1 and substrate protein. This assay was applied to all Taspase1 mutants as outlined below.

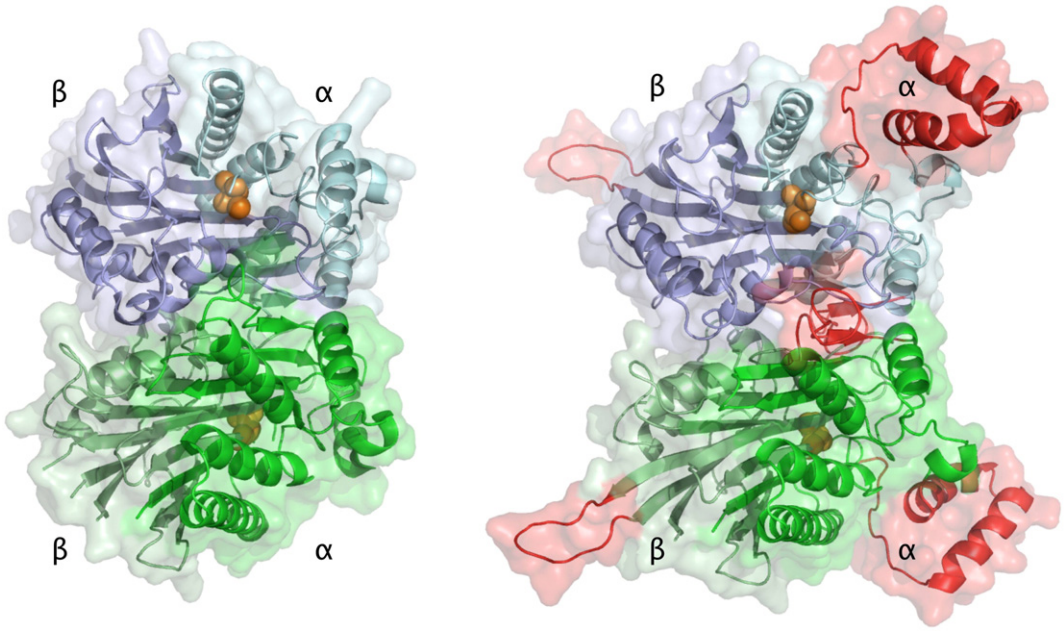

Fig. 1. Computer-aided modeling of Taspase1 based on the available crystal structure. Left: crystal structure of human Taspase1 (Khan et al., 2005). The PDB-structure 2A8J is displayed. Right: modeling of missing amino acid residues 206–229 and 352–362, and of a structural element formed by amino acid residues 164–180. This enabled us to modify the existing structure of Taspase1. Differences between the published crystal structure and the *in silico* remodeled Taspase1 structure are displayed in red. The catalytic T234 residues are displayed as orange spheres.

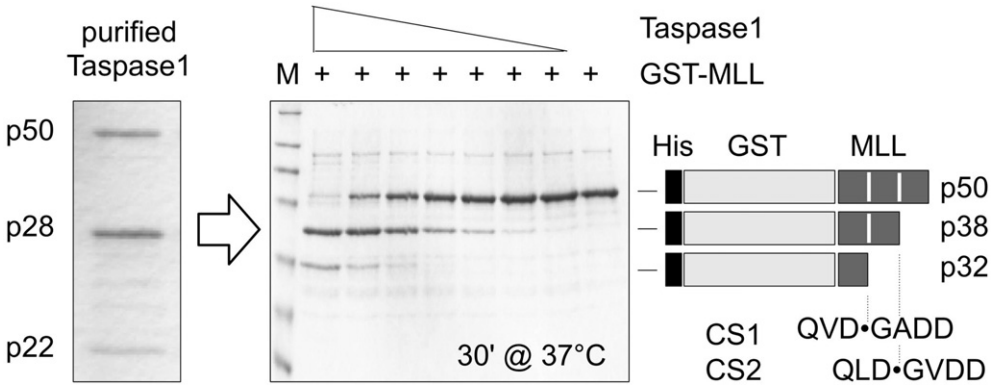

Fig. 2. *In vitro* Taspase1 enzyme assay. Left: affinity-purified Taspase1 protein from *E. coli*. Due to autoproteolysis, the p50 full-length protein is hydrolyzed into the p28 α- and the p22 β-subunits. Middle: a dilution experiment of recombinant Taspase1 in the presence of constant amounts of the GST–MLL substrate protein. M: protein marker. First lane: approximately 1 μg GST–MLL was coincubated with equimolar amounts of Taspase1 for 30 min at 37 °C. In subsequent lanes, the amount of Taspase1 was serially reduced by 2-fold. In the final dilution (1:128) no cleavage of the substrate protein could be observed. Right: scheme of the substrate protein that exhibits the cleavage sites CS1 and CS2, respectively; CS2 is the preferential cleavage site *in vitro* (p38), while CS1 represents a minor cleavage site (p32).

3.3. Site Directed Mutagenesis Reveals an Intrinsic Serine Protease-like Mechanism

Previous reports from our laboratory demonstrated that the AF4–MLL fusion protein requires Taspase1 to form a stable, oncogenic protein complex (Benedikt et al., 2011). The AF4–MLL complex was shown to be sufficient to initiate the development of acute lymphoblastic leukemia (ALL) in mice (Bursen et al., 2010). In the present study we addressed the following questions: (a) how important is the dimerization process for Taspase1 activity?; (b) which amino acids are involved in the autoproteolytic mechanism of the Taspase1 proenzyme?; and (c) how can we interfere with the enzymatic activity of Taspase1?

We focused on several candidate amino acid positions by visual inspection of the new model structure of Taspase1. First, amino acids in the vicinity of the two amino acid residues D233 and T234 were selected (Fig. 3A). The peptide bond between these residues needs to

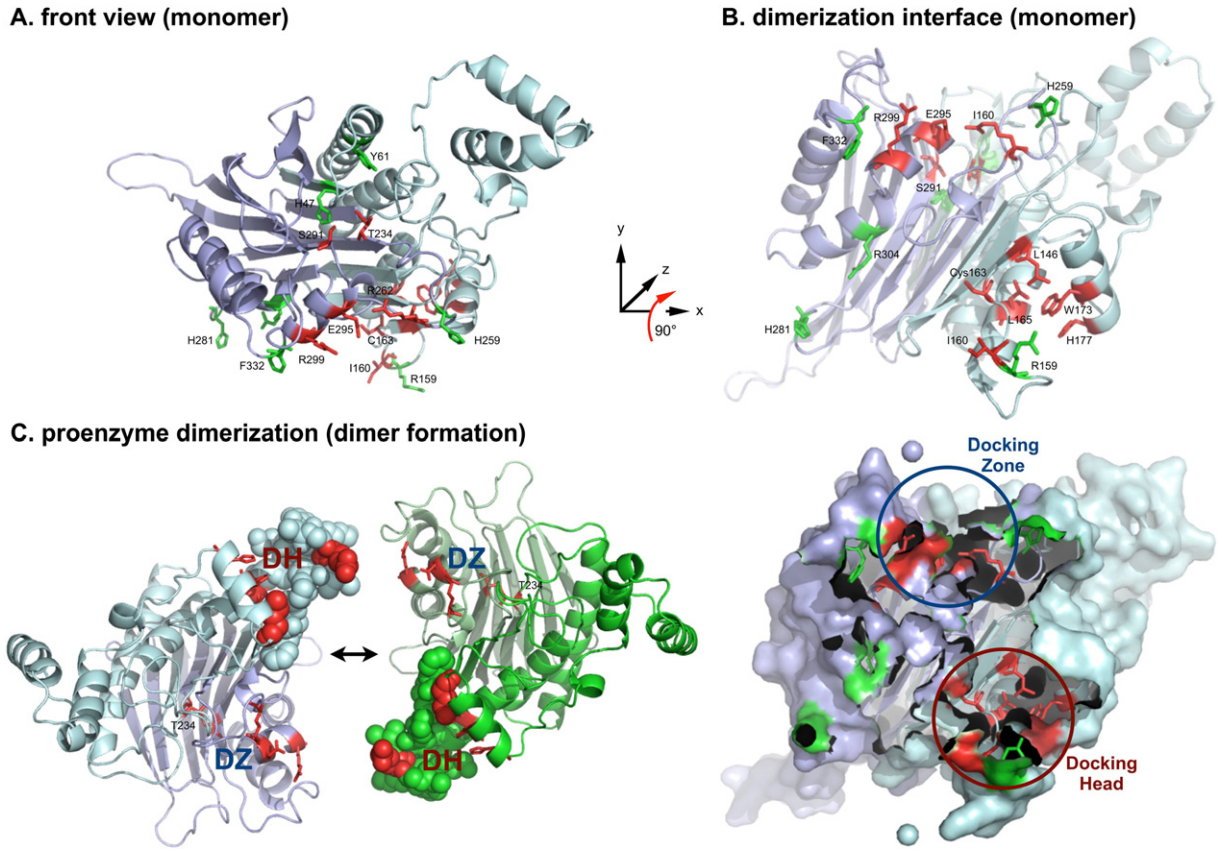

Fig. 3. Dissection of Taspase1 function by site-directed mutagenesis. A. Monomeric Taspase1 in front view (cartoon). B. Monomeric Taspase1 interaction interface. Top: cartoon view; bottom: surface view. Both the docking zone (DZ) and the docking head (DH) are indicated by circles. Mutated amino acid residues shown in green: no effect on dimerization, autoproteolysis or substrate hydrolysis; residues shown in red: disabled dimerization, autoproteolysis or substrate hydrolysis. C. Proenzyme dimerization process; monomeric Taspase1 proenzymes are displayed to show how their docking heads (DH) potentially bind to the corresponding docking zones (DZ) of the opposing monomer.

be hydrolyzed in order to obtain the active enzyme. In particular, we chose Y61, H47, and S291 for site-directed mutagenesis because they are localized near the D233/T234 dipeptide bond in the three-dimensional space. Secondly, we realized that both Taspase1 monomers display a large interaction interface containing several candidate amino acids (Fig. 3B). These are either able to form interactions by hydrogen bonds or by stacking interactions. The following interface amino acid residues were selected: I160, H259, H281, R304, R299 and F332. Thirdly, a 'docking head' became visible when each monomer was analyzed by its own (Fig. 3C; DH = docking head, DZ = docking zone). Selected amino acids are either localized in the 'docking zone' (E295 and R262) or within the docking head (V142, L146, R159, L165, W173, and H177). All these amino acids were subjected to site-directed mutagenesis. The resulting Taspase1 mutants were subsequently tested for: (a) their ability to form dimers; (b) their autoproteolytic activity; and (c) the ability to hydrolyze appropriate substrate protein.

As summarized in Fig. 3AB, mutations shown in green (Y61A, H47A, R159A, H259A, H281A, R304A, and F332A) had neither an effect on dimerization, autoproteolysis nor substrate cleavage. However, all amino acid positions displayed in red interfered with the proper function of Taspase1. The mutants T234D and S291A had obviously no autoproteolytic activity, and thus, were both unable to be converted into an active enzyme. While the T234D mutation was already published (Hsieh et al., 2003b), the importance of the S291 was not previously appreciated. A visual inspection of the enzymatic center suggested a potential mechanism for autoproteolysis, represented by the presence of a catalytic triad (H47, S291, and D233; see Suppl. Fig. S1A). However, the Taspase1 mutant H47A did not show any impairment of the autoproteolytic process. Thus, from our set of selected residues only S291 and D233 appear to be important for the autoproteolytic process. We also tested for the possibility that an N–O acyl shift mechanism is responsible for the autoproteolytic activity of Taspase1 (Perler, 1998). Such a mechanism was identified for another member of the threonine aspartase family member. Briefly, the glycosylasparaginase enzyme features a 'scissile peptide bond' between residue D151 and T152, which is autocatalytically hydrolyzed (Qian et al., 2003; Wang and Guo, 2010). The N–O acyl shift mechanism should be enhanced by the presence of 500 mM hydroxylamine, while the presence of 20 mM glycine should be inhibitory. However, no differences in the amount of proenzyme (p50) or the autoproteolytic peptides p28 and p22 were observed when compared to untreated Taspase1 (see Suppl. Fig. S1D). Thus, we concluded that autoproteolysis of Taspase1 apparently depends on S291 and D233, and not on a 'scissile peptide bond' as described for glycosylasparaginase. Scissile peptide bonds are normally characterized by a torsionally deformed amide (Wang and Guo, 2010), which is neither visible in the crystal structure nor in the new model of Taspase1.

Several other mutated amino acids — predominantly localized in the dimerization interface — had a profound effect on the function of Taspase1 (Fig. 3AB). Mutants R262A, E295A and R299E were all able

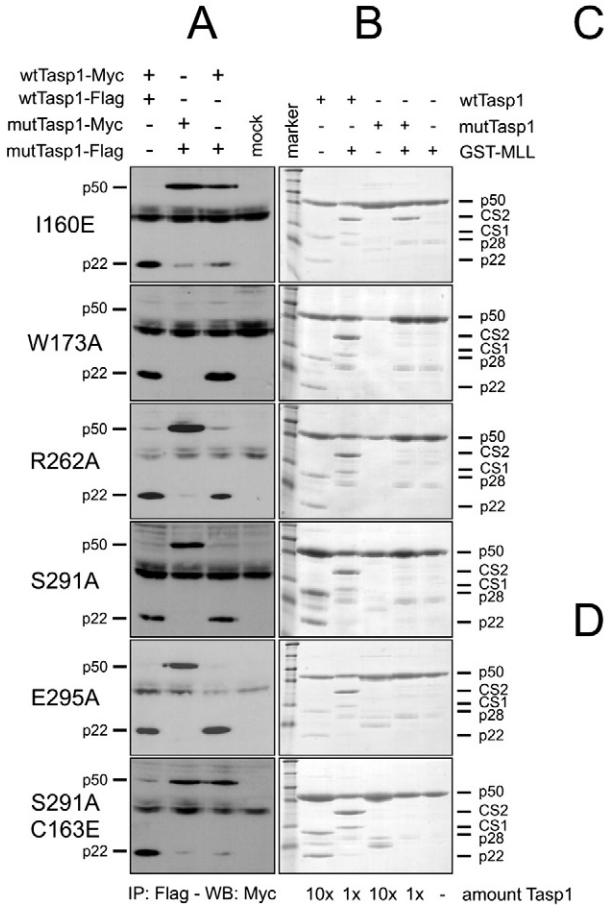

C

Taspase1 mutant	Dimerization	Autoproteolysis	Substrate hydrolysis
I160E	+	10%	NO
I160E / WT	+	30%	YES
C163E	+	NO	NO
C163 / WT	+	20%	NO
W173A	-	NO	NO
W173A / WT	+	100%	NO
T234D	+	NO	NO
T234D / WT	+	100%	NO
R262A	+	5%	NO
R262A / WT	+	90%	NO
S291A	+	NO	NO
S291A / WT	+	90%	NO
E295A	+	NO	NO
E295A / WT	+	95%	NO
R299E	+	NO	NO
R299E / WT	+	95%	NO
S291A/C163E	+	5%	NO
S291A/C163E / WT	+	5%	NO

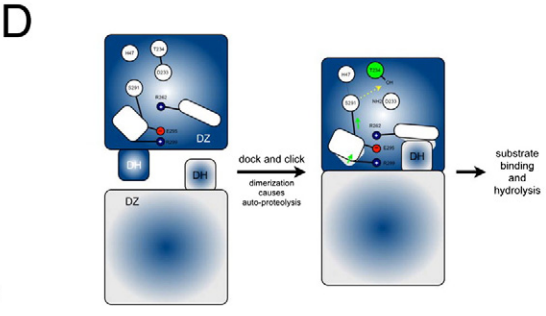

Fig. 4. Dimerization capability and *in vitro* hydrolysis activity of Taspase1 mutants. A. Co-immunoprecipitation experiments of Flag- and Myc-tagged Taspase1 expression constructs. For all experiments, Flag- and Myc-tagged Taspase1 variants were contransfected into HEK293T cells. After immunoprecipitation with anti-Flag-Tag antibody, all precipitates were probed with anti-Myc-Tag antibody. Lane 1: transfection of Taspase1-Myc and Taspase1-Flag; lane 2: transfection of mutated Taspase1-Myc and mutated Taspase-Flag; lane 3: transfection of Taspase1-Myc and mutant Taspase-Flag; lane 4: mock-control experiments. Detection of p22 fragment: dimerization and autoproteolysis occurs; detection of p50: dimerization occurs, while autoproteolysis is inhibited. B. SDS-Page of wildtype and mutant Taspase1 variants. Recombinant Taspase1 was loaded either alone (in a 10-fold higher concentration) or in combination with the GST–MLL substrate protein (1-fold). Left lanes: protein size marker. Lane 1: affinity-purified wildtype Taspase1 (p22, p28 and p50); lane 2: affinity-purified wildtype Taspase1 and GST–MLL substrate protein (CS1, CS2 and p50); lane 3: affinity-purified mutant Taspase1 (only p50); lane 4: affinity-purified mutant Taspase1 and GST–MLL substrate protein (only p50); lane 5: substrate GST–MLL protein (control; p50).

to dimerize, but the process of autoproteolysis and substrate hydrolysis was completely blocked (Fig. 4B). An exception was I160E, because this particular mutation was still able to dimerize, but autoproteolysis (Fig. 4A) and substrate hydrolysis was reduced (Fig. 4B). These data indicated that certain amino acid positions in the 'docking zone', *e.g.*, R299, E295 and R262, are important for triggering the autoproteolytic activity of Taspase1. In addition, the I160E mutation indicated that also the 'docking head' of the opposing monomer has relevance for this process. Both mutation clusters indicated for the first time, that the dimerization process of inactive Taspase1 monomers is of importance for the generation of enzymatically active Taspase1 dimers.

Another important 'docking head' mutation was the W173A Taspase1 mutant. This mutant was unable to form a homodimer, while mixing a wildtype with the W173A mutant still allowed dimerization, although to a much lesser extent (Fig. 4A). First, we assumed that the side-chain of W173 is able to form an arene–arene interaction with the H259 of the opposing Taspase1 monomer. However, the H259A mutation displayed no such effect. Then, the amino acid positions H177, L146, L165 and V142 were mutated into alanines. We tested various single and double mutants (Fig. 5A). The results of these experiments suggest that both L146 and L165 form a hydrophobic pocket for the W173 residue, while H177 presumably stabilizes the position of the W173 residue (Fig. 5B). Together these interactions may help to stabilize a distinct three-dimensional conformation of the 'docking head' in order to perform a 'dock and click' mechanism with an opposing Taspase1 monomer. As summarized in Fig. 5C, neither the W173A, the L146A/L165A nor the L146A/H177A mutants were able to form stable docking heads. As a consequence, none of these 3 mutants was able to dimerize. The V142A mutation served as a control and was not expected to have an effect on the docking head structure. In fact, this mutant did not impair the dimerization of Taspase1. Noteworthy, when the 'docking head' binds to its cognate docking zone in an opposing Taspase1 monomer, the most important amino acids affected by the dimerization process are again R262 and E295 (see below).

3.4. Dimerization is the Key Event to Activate an Intrinsic, Serine Protease-like Activation Mechanism

These results motivated us to inspect the docking zone of Taspase1 in more detail. When Taspase1 monomers bind to each other, both 'docking heads' bind near the catalytic center of the opposing monomer (docking zone). An example of a single 'docking zone' (blue) is displayed in Fig. 6. We propose that binding of the 'docking head' (green) leads to small changes in the opposing loop structure, resulting in a movement of R262 towards E295. E295 — normally attracted by the positive charge of R299 — would then move into the direction of the positively charged R262. Since E295 is directly linked to Ser291, this tiny movement of E295 may allow the correct positioning of S291 to initiate the essential autoproteolytic cleavage. Cleavage of the D233–T234 peptide bond would then activate the reactive center of Taspase1, which in turn would then allow substrate binding, and subsequently, the hydrolysis of bound substrate protein.

This proposed activation mechanism for Taspase1 proenzymes is supported by different experimental results: (a) we hypothesized that an R262A mutation should disable any movement of E295 towards R262, because of the missing positive charge. In fact, this particular mutation displayed no Taspase1 activity at all, while dimerization was not effected (Fig. 4AB); (b) similarly, an E295A mutation should also disable the movement of E295 towards R262, due the missing negative charge. Again, this single point mutation abolished any Taspase1 activity (Fig. 4AB); (c) finally, we hypothesized that a C163E mutation

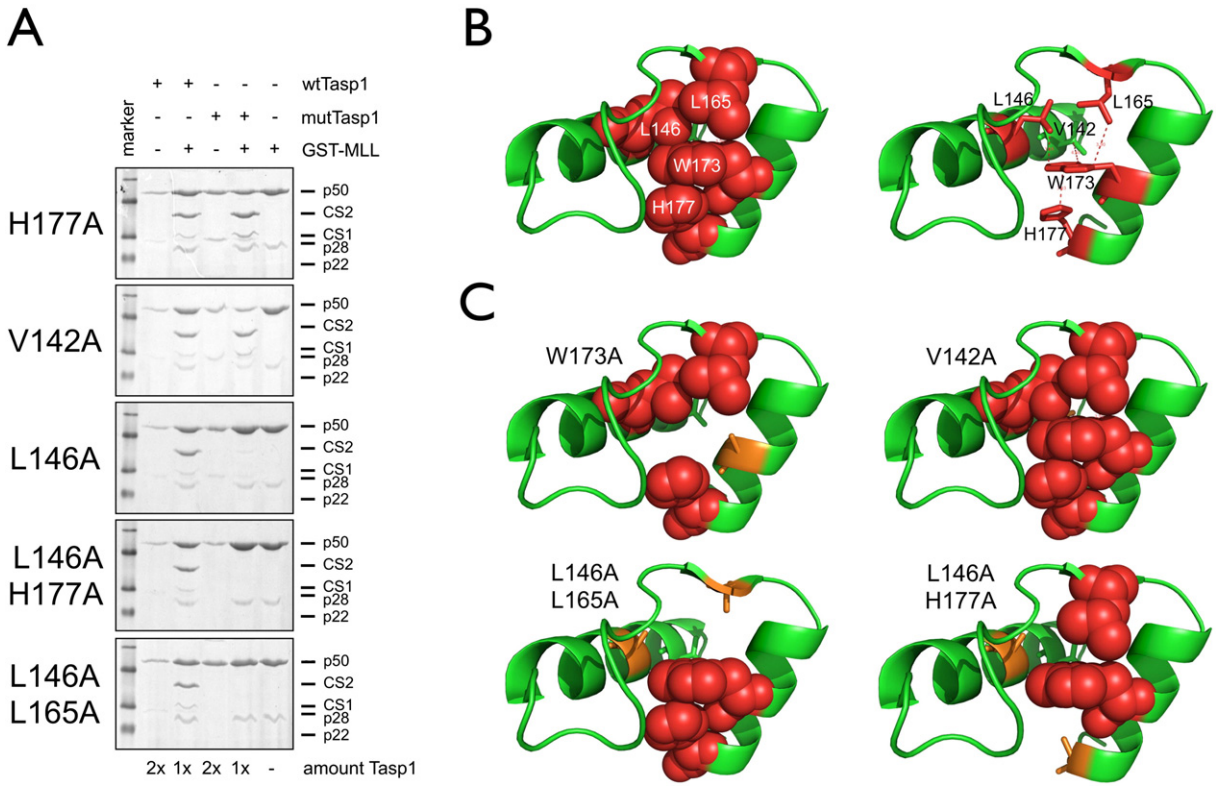

Fig. 5. Mutational analysis of the docking head. The W173A mutant of Taspase1 was shown to be dimerization deficient. In order to understand the function of W173, additional amino acids in the vicinity were mutated to alanines. A. Mutant Taspase1 variants were tested for their ability to dimerize and to hydrolyze the GST–MLL substrate protein. For details of the experiment see Fig. 4B. B. Wildtype Taspase1 docking head. Left: cartoon view with spheric view of all tested amino acids. Right: docking head in cartoon view with indicated distances between the tested amino acids. C. Mutant Taspase1 docking heads. W173A, L146A/L165A or L146A/H177A mutants were unable to dimerize. The control, V142A, did not display a dimerization deficiency.

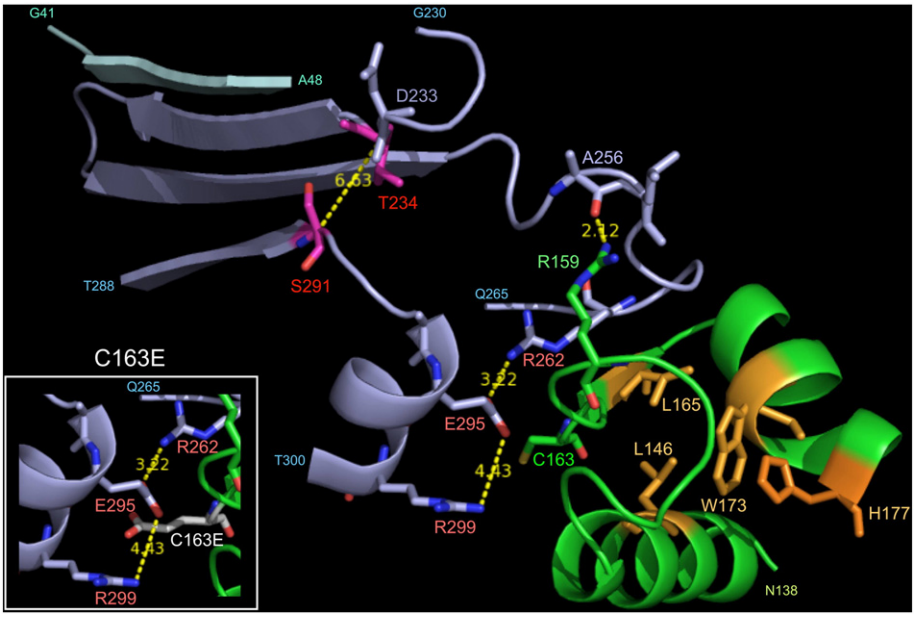

Fig. 6. Hypothetical mechanism of Taspase1 activation. Amino acids T286–T300 and G230–Q265 of Taspase1 represent the docking zone (blue colored). From the second Taspase1 monomer, only the docking head — represented by amino acids N138–H177 — is displayed (green colored). Important amino acid residues are indicated by a combination of a single letter and a number. Upon dimerization, the docking head binds to the docking zone. This causes a conformational change which enables R262 to attract residue E295. Subsequently, a tiny shift of E295 towards R262 causes the correct placement of S291, which then executes the autoproteolytic step (cleavage of peptide bond D233/T234). All distances are displayed in Angstrom. Inset: the consequences of the important C163E mutation are displayed. Upon dimerization with another Taspase1 monomer, the necessary movement of E295 towards R262 is presumably blocked due to a clash of negative charges.

within the docking head could create a clash of negative charges with E295 upon dimerization (see inset of Fig. 6). As a matter of fact, the C163E mutant was still able to dimerize (Fig. 4A), but completely blocked the step of autoproteolytic activation and substrate hydrolysis (Fig. 4B). These results imply that Taspase1 requires dimerization in order to become sequentially activated: dimerization causes a repositioning of S291, which in turn triggers the autoproteolytic step of the peptide bond between D233 and T234; the N-terminal T234 then becomes the catalytic center; substrate binding displaces the inhibitory chloride ion (Khan et al., 2005) and allows the repositioning of the T234 to finally perform the nucleophilic attack at the D^{1}–$G^{1'}$ peptide bond of a substrate protein bound to the catalytic center.

3.5. Establishment of the First Dominant-negative Taspase1 Variant (dnTASP1)

Based on these experimental results, we created the double mutant C163E/S291A. A S291A mutated monomer of Taspase1 is unable to become hydrolyzed between D233 and T234 upon dimerization with a wildtype Taspase1 monomer. Moreover, the C163E mutation within the 'docking head' (see inset of Fig. 6) interferes with the movement of E295 in the opposing monomer, and thus, blocks proper positioning of S291 in a co-bound wildtype Taspase1. Thus, binding of such a double-mutant to wildtype Taspase1 should lead to enzymatically inactive heterodimers, and substrate hydrolysis should not be observed. To test this hypothesis, wildtype Taspase1 (Myc-tagged) and the dnTASP1 (Flag-tagged) were co-transfected into HEK293T cells, and subsequently, co-immunoprecipitation experiments were performed. When mutant Taspase1 was precipitated and tested for co-bound wildtype Taspase1 (Fig. 4A), we observed mainly inactive Taspase1 (amount of p50) when compared to autoproteolytically cleaved wildtype Taspase1 dimers (amount of p22). In addition, no substrate cleavage was observed (Fig. 4B). Thus, we concluded that the Ser291A/C163E double mutant represents a dominant-negative mutant of Taspase1. We termed this double-mutant dnTASP1.

3.6. Functional Validation of Taspase1 Inhibition

dnTASP1 or wildtype Taspase1 expression plasmids were co-transfected with an AF4–MLL expression vector into HEK293T cells. Cellular lysates were tested for the presence of the AF4–MLL fusion protein. Full-length AF4–MLL (p328) is rapidly processed by Taspase1, resulting in generation of $p178^{N}$ and $p180^{C}$ protein fragments. Western blots were probed with the AF4·N antibody to detect the expected $p178^{N}$ fragment, as published (Bursen et al., 2004). As shown in Fig. 7A, the cleaved $p178^{N}$ protein fragment is visible in the presence of wildtype Taspase1, while no $p178^{N}$ protein fragment could be detected in the presence of dnTASP1. This is due to the fact that uncleaved AF4–MLL fusion protein is a substrate of SIAH1 and SIAH2 (Bursen et al., 2004), that mediates a very rapid poly-ubiquitinylation and proteasomal degradation of this oncoprotein. Only cleavage by Taspase1 allows the formation of a stable AF4–MLL fusion protein complex (Benedikt et al., 2011) that exerts the oncogenic properties (Bursen et al., 2010). Any interference with the formation of this stable complex leads to the rapid degradation of AF4–MLL (Pless et al., 2011).

In order to confirm this independently, we established an *in vivo* FRET biosensor assay that is based on BFP and GFP which are separated by the Taspase1 cleavage sites CS1 (AEGQVD·GADD) or CS2 (KISQLD·GVDD). This FRET biosensor was stably co-transfected either with empty vector (mock), wild-type Taspase1 (WT) or dnTASP1 (DN) into HEK293 cells. As shown in Fig. 7B, endogenous or transfected Taspase1 was not able to quench the BFP protein, while dnTASP1 did. The observed differences were highly significant ($p < 0.002$) and clearly demonstrated that in the presence of dnTASP1 normal Taspase1 activity is diminished. This leaves the FRET biosensor uncleaved and a strong quenching of BFP was the result (70% or 60% signal reduction at CS1 and CS2, respectively).

Next, we investigated the effects of dnTASP1 on *HOXA* gene transcription (Fig. 7C). Distinct *HOXA* genes (HOXA7, HOXA9 and HOXA10) are direct targets of the MLL protein complex. Expression of dnTASP1 expression had only subtle effects on *HOXA* gene transcription levels. However, *HOXA1* gene transcription was slightly increased,

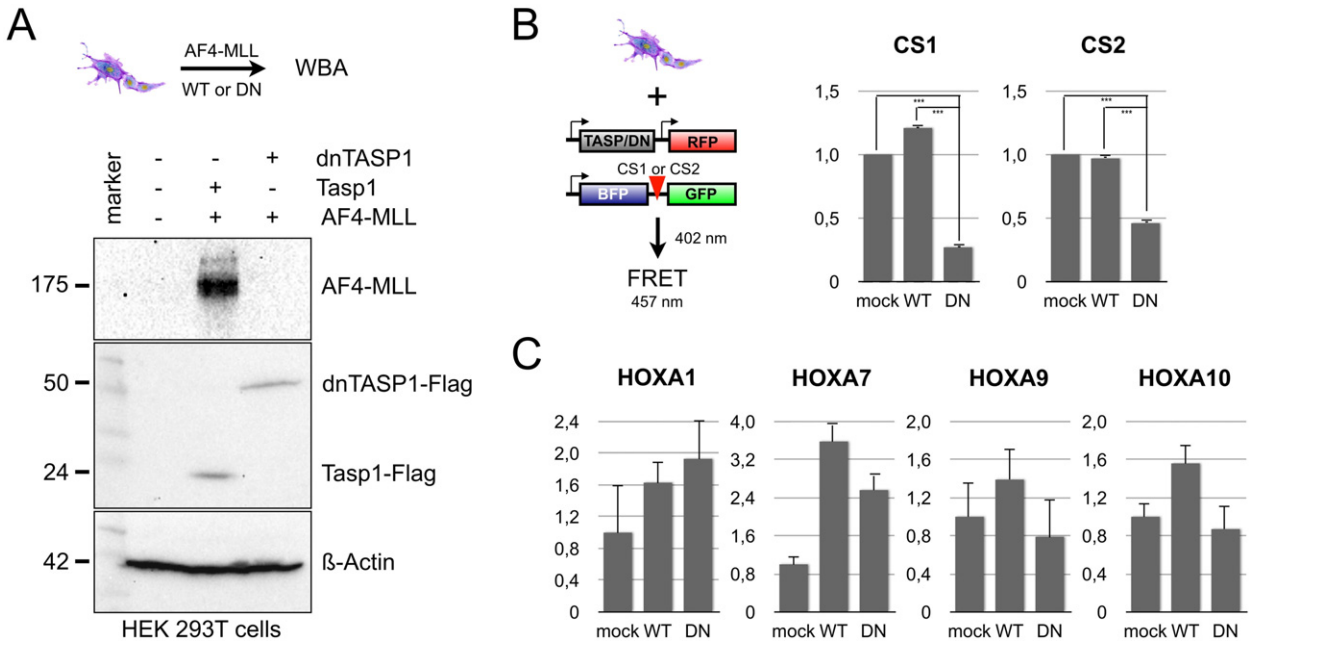

Fig. 7. Co-expression of FRET reporter or AF4–MLL with dnTASP1. A. Western blot experiments were performed after co-expression of AF4–MLL with wildtype Taspase1 or dnTASP1. Detection of cleaved AF4–MLL fusion protein is shown on top. The presence of wildtype Taspase1 or dnTASP1 was confirmed with an antiserum that detects the C-terminal Flag-Tag of Taspase1 (p24) or of the uncleaved dnTASP1 mutant (p50). Protein loading controls were probed with an antiserum against β-actin. B. *In vivo* FRET assay. HEK293 cells were stably transfected with the FRET biosensor in combination with empty vector (mock), wild-type Taspase1 (WT) or the dominant-negative Taspase1 mutant (DN). When Taspase cleavage sites are cleaved then the energy transfer between BFP and GFP is not quenched. However if the cleavage sites are not cleaved by dnTASP1, quenching occurs which results in a lower absorbance at 457 nm. C. Real-time PCR experiments performed for certain *HOXA* genes. Untransfected cells served as negative control. Several of the tested *HOXA* genes are differentially expressed in the presence of dnTASP1.

while that one of *HOXA7*, *HOXA9* and *HOXA10* was slightly reduced in the presence of dnTASP1. These subtle effects are due to the fact that Taspase1-unprocessed MLL protein is still able to steer transcription of these target genes (Hsieh et al., 2003b). This is important because it demonstrates that knocking down endogenous Taspase1, and thus also the functions of endogenous MLL, does not significantly impair normal cell physiology. By contrast, interfering with functions provided by Taspase1 in the context of the AF4–MLL oncoprotein leads to the

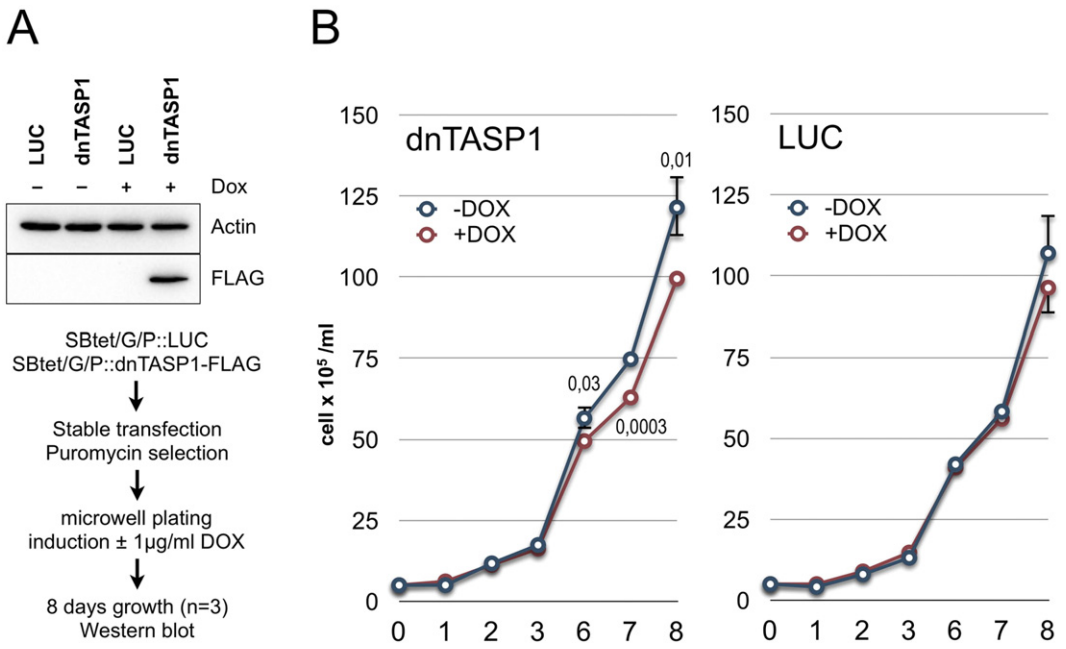

Fig. 8. Expression dnTASP1 in t(4;11) SEM cells. SEM cells were stably transfected with Sleeping Beauty vectors (SBtet/GFP/Puro vectors) that either express Luciferase (LUC; negative control) or the dnTASP1 in a doxycyclin-inducible manner. Transgenic cells were selected and all experiments were performed with cells that uniformly express GFP. A. Western blot experiments were performed 8 days after induction to validate the expression of the inducible Flag-Tagged dnTASP1. B. Cell growth was measured on days 0, 1, 2, 3, 6, 7 and 8. Cell counts are displayed as X cells × 10^5 cells/ml. Cells expressing dnTASP1 (left panel) or LUC (right panel) are displayed with and without induction by 1 µg/ml doxycyclin. DnTASP1-expressing SEM cells displayed a significant difference in their cell numbers starting on day 6 (p-values are indicated for days 6, 7 and 8). This was not the case with Luciferase-expressing SEM cells, where error bars overlapped at day 8. All experiments were repeated in independent experiments (n = 3). Mean values and standard deviations of these 3 experiments are shown. SD was only indicated when applicable.

disappearance of the leukemia-inducing AF4–MLL fusion protein, and thus, should have a dramatic effect for t(4;11) leukemia cells.

Finally, we stably transfected t(4;11)-positive SEM cells by using our recently established Sleeping Beauty vector technology (Kowarz et al., 2015). We used a control vector with cloned Luciferase, and another vector with Flag-tagged dnTASP1. SEM cells were selected over 4 weeks to obtain two homogenous cell populations that all expressed the GFP marker deriving from the vector backbone. Cells were then seeded and induced for the expression of their transgenes (Fig. 8A). The cell population of Luciferase-expressing SEM cells did not differ in their growth behavior when compared to the non-induced control (see Fig. 8B, right panel), but cells expressing dnTASP1 did show a reproducible and significant growth difference already after several days. This was reproducible in three consecutive experiments (see Fig. 8B, left panel). This was a first indication, that dnTASP1 may indeed impair functions deriving from the AF4–MLL fusion protein which then resulted in impaired cell growth. We also analyzed the cell cycle of those cells and observed a prolonged G0/1 phase after releasing from a double-thymidine block (data not shown). This finding may explain the observed effect on cell growth, but further studies will be necessary to investigate these findings in more detail.

4. Discussion

In the context of t(4;11) leukemia, Taspase1 is a conditional oncoprotein because it mediates the proteolysis of the AF4–MLL fusion protein (p328). The resulting protein fragments ($p178^N$ and $p180^C$) form a heterodimer which resembles a molecular platform for the assembly of the highly stable AF4–MLL multiprotein complex. This high molecular weight complex exerts an enhanced P-TEFb activity and causes ectopic histone signatures (Benedikt et al., 2011). Retroviral expression of the AF4–MLL fusion protein in murine hematopoietic stem/precursor cells caused the development of proB ALL in mice (Bursen et al., 2010). Consequently, we decided to investigate Taspase1 at the molecular level, aiming to understand the functional relationship between Taspase1 and AF4–MLL, and to translate this knowledge into novel strategies aiming to block the oncogenic functions deriving from AF4–MLL.

First, we refined the available crystal structure of human Taspase1 by *in silico* modeling and used this structural model of Taspase1 to identify critical amino acid residues. Based on our data, dimerization of two Taspase1 monomers seems to be a key step for activating the intrinsic autoproteolytic function (Fig. 6). There are several important amino acids, but S291 and D233 are critical for the hydrolysis of the peptide bond between residues D233 and T234. This is in line with recent findings obtained for several proteases, demonstrating that a single serine residue is sufficient to cause autoproteolytic activity (Polgár, 2005). The T234 residue apparently remains in an inactive conformation due to the presence of a chloride ion, which is coordinated by the peptide backbone of G49, N100 and T234. This chloride anion functions as a reversible competitive inhibitor at physiological chloride concentrations (IC_{50} ~ 25 mM NaCl) (Khan et al., 2005). Binding of a cognate substrate leads to the displacement of the inhibitory chloride anion, possibly by using the carboxyl moiety of $D^{4'}$ deriving from the consensus cleavage site ($Q^3[F,I,L,V]^2D^1|G^{1'}X^{2'}X^{3'}D^{4'}$). As already described by Khan et al. (2005) the displacement of the chloride ion allows T234 to rotate by approximately 180° into the appropriate position to perform the nucleophilic attack at the peptide bond between D^1 and $G^{1'}$ of bound substrate protein. This explains, why many efforts aiming to identify a potent lead which targets the enzymatic center of Taspase1 remained so far without success.

In order to develop new drug strategies against Taspase1, we used the approach to mutagenize Taspase1, and to use these mutant variants of Taspase1 in functional experiments. These experiments revealed that inactive Taspase1 monomers use a 'docking head' to bind into a 'docking zone' of an opposing Taspase1 monomer. This 'dock-and-click' mechanism appears to be a prerequisite for the functional activation of Taspase1, because mutations within the docking head (W173A, L146A/L165A, and L146A/H177A; I160E and C163E) or the corresponding docking zone (R262A, E295A and R299E) abolished the pro- and enzymatic activities of Taspase1.

The knowledge about Taspase1 and its particular activation mechanism was subsequently used to design a dominant-negative variant of Taspase1 (dnTASP1). This mutant combines the S291A and C163E mutations. Therefore, such a mutant monomer — *per se* unable to become activated itself — binds with the modified docking head to other Taspase1 monomers and thereby blocks the autoproteolytic step. Co-immunoprecipitation and *in vitro* experiments revealed that neither dnTASP1 homodimers nor dnTASP1::Taspase1 heterodimers display any autoproteolytic or substrate hydrolysis activity (Fig. 4AB).

DnTASP1 should represent *per se* a therapeutic protein in the context of t(4;11) leukemia, because the co-expression of dnTASP1 together with the leukemogenic AF4–MLL oncoprotein resulted in the disappearance of the unprocessed AF4–MLL fusion protein (Fig. 7A). This is due to the fact that unprocessed AF4–MLL fusion protein (p328) is a substrate of the two E3-ligases SIAH1 and SIAH2. Both E3 ligases mediate polyubiquitinylation, which in turn leads to a rapid proteasomal degradation of the AF4–MLL oncoprotein (Bursen et al., 2004). By contrast, Taspase1-hydrolyzed AF4–MLL ($p178^N$ and $p180^C$) forms a heterodimer which serves as a platform for the assembly of a high molecular weight complex that is highly stable and leukemogenic (Benedikt et al., 2011). We attempted to validate this hypothesis by analyzing the effects of dnTASP1 on cells that bear a t(4;11) translocation. For this purpose, we used our recently established Sleeping Beauty vectors to transfect SEM cells (Kowarz et al., 2015). After a 4 week period of 'pulsed selection' to obtain transgenic SEM cells, we analyzed the two transgenic cell populations for their growth behavior. The induction of the dnTASP1 transgene led to a significant and reproducible reduction of cell growth in a doxycyclin-dependent manner (Fig. 8), while control experiments (Luciferase) did not reveal such effects. These data are supporting our notion about the role of dnTASP1 for AF4–MLL.

Taspase1 is presumably not only important in the context of normal MLL functions or leukemia, but also for solid tumors. Several cell lines deriving from different solid tumors overexpress Taspase1 (Takeda et al., 2006). This suggests that Taspase1 has a potential function in tumor cells although only *MLL* germline alleles are expressed. Solid tumors may require more cleaved MLL complexes *e.g.*, to enhance transcriptional processes. This important concept has been recently successfully validated for breast cancer cells (Dong et al., 2014).

Several groups — including our own — have already tried to identify potential Taspase1 inhibitors (Lee et al., 2009; Chen et al., 2012). However, all these screening strategies failed so far. The reason for this is not quite clear but may be due to the inhibitory chloride anion that disables Taspase1 in the absence of substrate. Conversely, our data imply to use an allosteric inhibition approach in order to target Taspase1 by small molecules. Taspase1 could potentially be inhibited by targeting the 'docking zone', *e.g.*, by blocking the movement of the E295 residue. However, such experiments would require to crystallize Taspase1 monomers (*e.g.*, the W173A mutant). Since there is no guarantee for good crystals, we suggest to use our established *in vivo* FRET reporter assay for initial screening experiments. Since this cellular system may respond to any kind of Taspase1 inhibition, it will presumably speed up any kind of screening effort to identify first lead structures.

In conclusion, we provide molecular evidence for a sequential activation mode of Taspase1 upon dimerization. This process is based on a 'click-and-dock' mechanism between Taspase1 monomers. Mutations in the 'docking head' or 'docking zone' disable Taspase1 activities, indicating that Taspase1 can be inhibited by an allosteric mechanism. This knowledge could be directly translated into efforts to develop Taspase1 inhibitors by using the tools established throughout this work.

Author Contributions

SS and CE have performed experiments; TG has performed the MD simulation to provide the new Taspase1 structure; EK, GS and RM have designed all experiments; RM has written the manuscript; and GS has edited the manuscript.

Funding

This study was supported by grant DKS 2011.09 from the German Children Cancer Aid to RM, and by research grants Ma1876/10-1 and Ma1876/11-1 from the DFG to RM. RM is PI within the CEF on Macromolecular Complexes funded by DFG grant EXC 115.

Role of Funding Resources

No funders played a role in study design, data collection, data analysis, interpretation or writing the report.

Conflict of Interest

We declare that we have no conflict of interest.

Acknowledgements

The authors wish to thank Alessa Kühn for establishing the method to stably transfect t(4;11) SEM cells.

Appendix A. Supplementary Data

Supplementary data to this article can be found online at http://dx.doi.org/10.1016/j.ebiom.2015.04.009.

References

Benedikt, A., Baltruschat, S., Scholz, B., et al., 2011. The leukemogenic AF4–MLL fusion protein causes P-TEFb kinase activation and altered epigenetic signatures. Leukemia 25 (1), 135–144.

Bursen, A., Moritz, S., Gaussmann, A., Moritz, S., Dingermann, T., Marschalek, R., 2004. Interaction of AF4 wild-type and AF4·MLL fusion protein with SIAH proteins: indication for t(4;11) pathobiology? Oncogene 23 (37), 6237–6249.

Bursen, A., Schwabe, K., Rüster, B., et al., 2010. AF4–MLL is capable of inducing ALL in mice without requirement of MLL–AF4. Blood 115 (17), 3570–3579.

Chen, D.Y., Lee, Van Tine, B.A., et al., 2012. A pharmacologic inhibitor of the protease Taspase1 effectively inhibits breast and brain tumor growth. Cancer Res. 72 (3), 736–746.

Dong, Y., Van Tine, B.A., Oyama, T., Wang, P.I., Cheng, E.H., Hsieh, J.J., 2014. Taspase1 cleaves MLL1 to activate cyclin E for HER2/neu breast tumorigenesis. Cell Res. 24 (11), 1354–1366.

Dou, Y., Milne, T.A., Tackett, A.J., et al., 2005. Physical association and coordinate function of the H3 K4 methyltransferase MLL1 and the H4 K16 acetyltransferase MOF. Cell 121 (6), 873–885.

Eswar, N., Webb, B., Marti-Renom, M.A., et al., 2006. Comparative protein structure modeling using Modeller. Curr. Protoc. Bioinformatics (Chapter 5, Unit 5.6).

Evan, G.I., Lewis, G.K., Ramsay, G., Bishop, J.M., 1985. Isolation of monoclonal anitibodies specific for human c-myc proto-oncogene product. Mol. Cell. Biol. 5 (12), 3610–3616.

Gan, T., Jude, C.D., Zaffuto, K., Ernst, P., 2010. Developmentally induced Mll1 loss reveals defects in postnatal haematopoiesis. Leukemia 24 (10), 1732–1741.

Guenther, M.G., Jenner, R.G., Chevalier, B., et al., 2005. Global and Hox-specific roles for the MLL1 methyltransferase. Proc. Natl. Acad. Sci. U. S. A. 102 (24), 8603–8608.

Hopp, T.P., Prickett, K.S., Price, V.L., et al., 1988. A short polypeptide marker sequence useful for recombinant protein identification and purification. Nat. Biotechnol. 6, 1204–1210.

Hsieh, J.J., Cheng, E.H., Korsmeyer, S.J., 2003a. Taspase1: a threonine aspartase required for cleavage of MLL and proper HOX gene expression. Cell 115 (3), 293–303.

Hsieh, J.J., Ernst, P., Erdjument-Bromage, H., Tempst, P., Korsmeyer, S.J., 2003b. Proteolytic cleavage of MLL generates a complex of N- and C-terminal fragments that confers protein stability and subnuclear localization. Mol. Cell. Biol. 23 (1), 186–194.

Jin, S., Zhao, H., Yi, Y., Nakata, Y., Kalota, A., Gewirtz, A.M., 2010. c-Myb binds MLL through menin in human leukemia cells and is an important driver of MLL-associated leukemogenesis. J. Clin. Invest. 120 (2), 593–606.

Jude, C.D., Climer, L., Xu, D., Artinger, E., Fisher, J.K., Ernst, P., 2007. Unique and independent roles for MLL in adult hematopoietic stem cells and progenitors. Cell Stem Cell 1 (3), 324–337.

Khan, J.A., Dunn, B.M., Tong, L., 2005. Crystal structure of human Taspase1, a crucial protease regulating the function of MLL. Structure 13 (10), 1443–1452.

Kowarz, E., Burmeister, T., Lo Nigro, L., et al., 2007. Complex MLL rearrangements in t(4;11) leukemia patients with absent AF4·MLL fusion allele. Leukemia 21 (6), 1232–1238.

Kowarz, E., Löscher, D., Marschalek, R., 2015. Optimized Sleeping Beauty transposons rapidly generate stable transgenic cell lines. Biotechnol. J. 10 (4), 647–653.

Krivtsov, A.V., Feng, Z., Lemieux, M.E., et al., 2008. H3K79 methylation profiles define murine and human MLL–AF4 leukemias. Cancer Cell 14 (5), 355–368.

Laskowski, R.A., MacArthur, M.W., Moss, D.S., Thornton, J.M., 1993. PROCHECK — a program to check the stereochemical quality of protein structures. J. Appl. Crystallogr. 26, 283–291.

Lee, J.T., Chen, D.Y., Yang, Z., Ramos, A.D., Hsieh, J.J., Bogyo, M., 2009. Design, syntheses, and evaluation of Taspase1 inhibitors. Bioorg. Med. Chem. Lett. 19 (17), 5086–5090.

Mátés, L., Chuah, M.K., Belay, E., et al., 2009. Molecular evolution of a novel hyperactive Sleeping Beauty transposase enables robust stable gene transfer in vertebrates. Nat. Genet. 41 (6), 753–761.

McMahon, K.A., Hiew, S.Y., Hadjur, S., et al., 2007. Mll has a critical role in fetal and adult hematopoietic stem cell self-renewal. Cell Stem Cell 1 (3), 338–345.

Meyer, C., Kowarz, E., Hofmann, J., et al., 2009. New insights into the *MLL* recombinome of acute leukemias. Leukemia 23 (8), 1490–1499.

Michalska, K., Bujacz, G., Jaskolski, M., 2006. Crystal structure of plant asparaginase. J. Mol. Biol. 360 (1), 105–116.

Nakamura, T., Mori, T., Tada, S., et al., 2002. ALL-1 is a histone methyltransferase that assembles a supercomplex of proteins involved in transcriptional regulation. Mol. Cell 10 (5), 1119–1128.

Ono, R., Nosaka, T., Hayashi, Y., 2005. Roles of a trithorax group gene, MLL, in hematopoiesis. Int. J. Hematol. 81 (4), 288–293.

Perler, F.B., 1998. Protein splicing of inteins and hedgehog autoproteolysis: structure, function, and evolution. Cell 91 (1), 1–4.

Pless, B., Oehm, C., Knauer, S., Stauber, R.H., Dingermann, T., Marschalek, R., 2011. The heterodimerization domains of MLL — FYRN and FYRC — are potential target structures in t(4;11) leukemia. Leukemia 25 (4), 663–670.

Polgár, L., 2005. The catalytic triad of serine peptidases. Cell. Mol. Life Sci. 62 (19–20), 2161–2172.

Qian, X., Guan, C., Guo, H.C., 2003. A dual role for an aspartic acid in glycosylasparaginase autoproteolysis. Structure 11 (8), 997–1003.

Takeda, S., Chen, D.Y., Westergard, T.D., et al., 2006. Proteolysis of MLL family proteins is essential for taspase1-orchestrated cell cycle progression. Genes Dev. 20 (17), 2397–2409.

Wächter, K., Kowarz, E., Marschalek, R., 2014. Functional characterisation of different MLL fusion proteins by using inducible Sleeping Beauty vectors. Cancer Lett. 353 (2), 196–202.

Wang, Y., Guo, H.C., 2010. Crystallographic snapshot of glycosylasparaginase precursor poised for autoprocessing. J. Mol. Biol. 403 (1), 120–130.

Wilkinson, A.C., Ballabio, E., Geng, H., et al., 2013. RUNX1 is a key target in t(4;11) leukemias that contributes to gene activation through an AF4–MLL complex interaction. Cell Rep. 3 (1), 116–127.

Yokoyama, A., Cleary, M.L., 2008. Menin critically links MLL proteins with LEDGF on cancer-associated target genes. Cancer Cell 14 (1), 36–46.

Yokoyama, A., Kitabayashi, I., Ayton, P.M., Cleary, M.L., Ohki, M., 2002. Leukemia proto-oncoprotein MLL is proteolytically processed into 2 fragments with opposite transcriptional properties. Blood 100 (10), 3710–3718.

Yokoyama, A., Wang, Z., Wysocka, J., et al., 2004. Leukemia proto-oncoprotein MLL forms a SET1-like histone methyltransferase complex with menin to regulate Hox gene expression. Mol. Cell. Biol. 24 (13), 5639–5649.

Zhou, H., Spicuglia, S., Hsieh, J.J., et al., 2006. Uncleaved TFIIA is a substrate for taspase 1 and active in transcription. Mol. Cell. Biol. 26 (7), 2728–2735.